Pure appl. geophys. 162 (2005) 221–248
0033–4553/05/020221–28
DOI 10.1007/s00024-004-2598-y

Pure and Applied Geophysics

Subsidence and Sinkhole Hazard Assessment in the Southern Dead Sea Area, Jordan

DAMIEN CLOSSON[1], NAJIB ABOU KARAKI[2], YANN KLINGER[3], and MUSA JAD HUSSEIN[4]

Abstract—The Dead Sea area is increasingly facing serious subsidence and sinkhole hazards. On March 22, 2000, the dyke of a two-month old major salt evaporation pond, located along the shore of the Lisan Peninsula (Jordan), collapsed over almost two kilometers. The pond was set up over unstable new lands that have been progressively emerging during the last three decades. In one hour, 56 millions m^3 of brine poured out into the northern, natural part of the Sea. Here, we present data suggesting that the drop of the water level, in conjunction with the particular tectonic setting of this area, is at least one of the factors that led to the disaster. We focused our study over the northern part of the Lisan Peninsula and Ghor Al Haditha which are two places undergoing the most intense deformations along the Jordanian Dead Sea coast. We used the results of a static high precision gravimetric survey to detect subsurface cavities in Ghor Al Haditha. We analyzed a interferometric digital terrain model of the recent emerged platform of the Lisan peninsula and interpreted radar differential interferograms contemporary with gravity measurements for the peninsula. We discuss the possibilities to detect, assess and monitor areas prone to collapse on the Jordanian side of the southern Dead Sea coast.

Key words: Radar differential interferometry, gravimetry, subsidence, sinkhole, Dead Sea, Jordan.

1. Introduction

The Dead Sea Basin (DSB) is the lowest place on the Earth. The watershed of this terminal lake has a surface of 40650 km^2 (USGS, 1998). It receives a mean annual precipitation that varies from 1200 mm in the north to less than 50 mm in the south (USGS, 1998). For four decades, running and ground waters have been intensely exploited by the Israelis (National Water Carrier, Dead Sea Works) and the

[1] Centre Spatial de Liège, Université de Liège. Avenue Pré Aily, B4031, Angleur, Belgique. Post exchange at: Royal Military Academy, Signal and Image Center, avenue de la Renaissance, 30, B-1000 Brussels. Belgium. E-mail: dclosson@rma.ac.be

[2] Department of Applied and Environmental Geology, University of Jordan, 11942 Amman. Jordan. E-mail: naja@ju.edu.jo

[3] Laboratoire de Tectonique - UMR7578, Boite 89, Institut de Physique du Globe. 75252 Paris cedex 05, France. E-mail: klinger@ipgp.jussieu.fr

[4] Earth and Environmental Science Department, Yarmouk University, Irbed-Jordan. E-mail: musajad4@yahoo.com

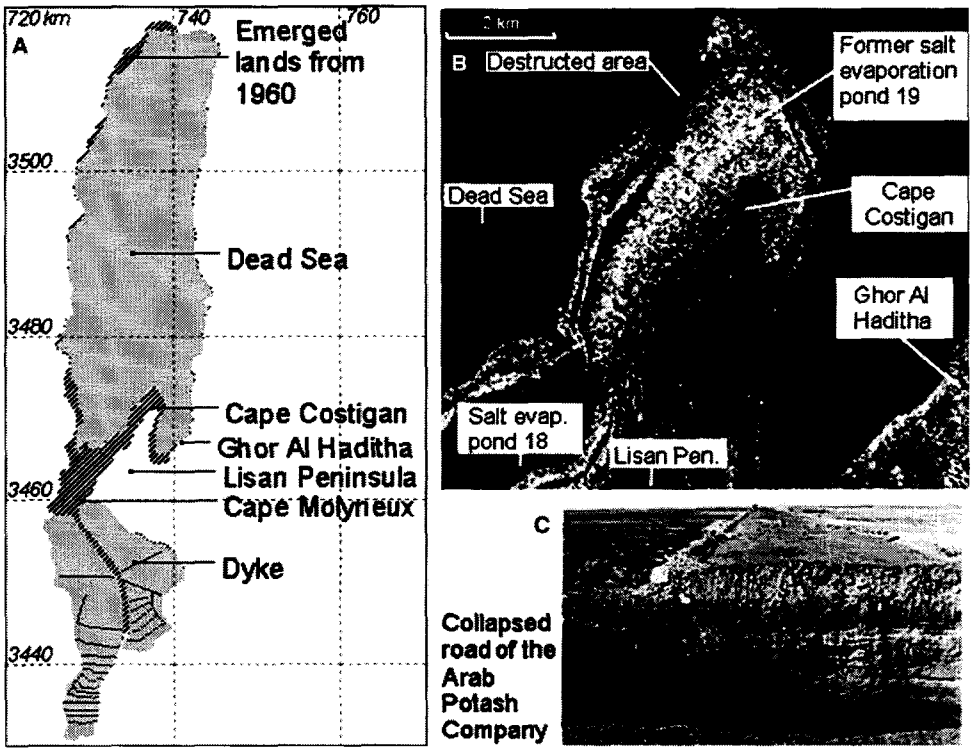

Figure 1

A. Dead Sea location map (UTM 36, WGS 84). Notice that the emerged areas during the last forty years include the hatched surfaces on the figure plus all the Dead Sea area situated south of Cap Molyneux which is nowadays only artificially covered with pumped Dead Sea water for industrial purposes (Potash extraction). B. The ERS-2 subset image, ascending, orbit 34494 frame 621, November 24th, 2001, shows the northern part of the Lisan Peninsula. The NW shore was partly amputated after the collapse of a segment of the dyke's SEP 19 and the emptying of 56 millions of m^3 brine into the Dead Sea in only one hour. The accident occurred on March 22, 2000. C. Sinkholes affected infrastructures such as roads. The diameter exceeded 10 meters.

Jordanians (East Ghor Canal, Arab Potash Company (APC)) resulting in a strong imbalance in the water budget of the Dead Sea (DS). SALAMEH and ABU NASEIR (1999), SALAMEH and EL-NASER (1999) and SALAMEH and EL-NASER (2000) recorded an annual deficit of around 1000 million m^3 with respect to the situation in the mid-sixties. Consequently, new unstable lands emerged progressively. At the end of seventies, the Lynch Strait emerged and separated the DS into northern and southern basins (Fig. 1A). The water level has been dropping from about 392 m below sea level (bsl) in 1950 to 416.3 m bsl by December 2002 (APC, written communication). The level has strongly fluctuated through the Quaternary period due to long-term climatic and tectonic causes (NIEMI and BEN AVRAHAM, 1997). The present rapid decrease,

however, is mainly induced by human activities and is unique in the whole history of the DS (SALAMEH and ABU NASEIR, (1999); SALAMEH and EL-NASER, (1999); and SALAMEH and EL-NASER 2000).

Contemporary with the sharp drop of the water table from the sixties, the areas of Ghor Al Haditha (GAH) and the Lisan Peninsula (LP), Jordan (Fig. 1A), were particularly affected by sinkholes and other metric to kilometric subsidence related phenomena. They are affecting fields, plantations, houses, roads, salt evaporation ponds (SEP) and industrial dykes (Figs. 1B, C; Fig. 5).

During the nineties, the APC progressively extended its industrial complex of SEP over the unstable Recent Emerged Platform (REP). Those new lands (Fig. 1) encircle the peninsula emerged before 1960 (hereafter we call it the 'old' part). A decametric sea-cliff separates the 'old' and recent areas of the LP. In October 1992, near Cape Molyneux, a road collapsed over about 100 m (KNIGHT, 1993; TAQIEDDIN *et al.*, 2000; TAPPONNIER, 1993). The destroyed area should become part of the 20 km^2 SEP 18 built in 1994. The company decided to move the pond a few hundred meters eastward. In October 2002, the SEP 18 was partially dried up because of the appearance of new sinkholes wide enough to threaten its stability.

A more serious case is that of the SEP 19. Built at the end of the nineties, for about 30 million US$, it was designed to contain 75 million m^3 of brine (AL ARAB AL YAWM, 2001). On March 22, 2000, a part of its dyke collapsed over 1650 m. The destruction took place two kilometers NW of the Cape Costigan (Fig. 1 B). Consequently, when the dyke collapsed, 56 million m^3 of brine poured out into the northern, natural part of the DS, increasing the water level of about 10 cm in less than one hour (APC, personal communication). The destroyed zone is clearly visible on satellite images posterior to the collapse (Fig. 1B).

Sinkholes most generally result from the upward sub-vertical movement of cavities that developed because of the dissolution of underlying salt layers (ARKIN and GILAT, 2000; TAQIEDDIN *et al.*, 2000). As a consequence of the DS falling, the interface between the DS water and the ground water is falling too. The salt layers, previously surrounded by saturated water in respect to salt, are now exposed to aggressive dissolution by unsaturated ground water.

Subsidence phenomena affect the DS shore. This subsidence appears to be structurally controlled by faults, seaward landslides, and salt domes (BAER *et al.*, 2002).

In the present study, we analyze outputs from ERS (European Remote Sensing satellite) synthetic aperture radar interferometry (InSAR) and differential interferometry (DInSAR) in relation with results from precise gravity measurements and more than ten years of field investigations in the LP and GAH. We discuss the possibilities to detect, assess and monitor prone collapse areas in this changing hazardous environment of the Jordanian Dead Sea coast.

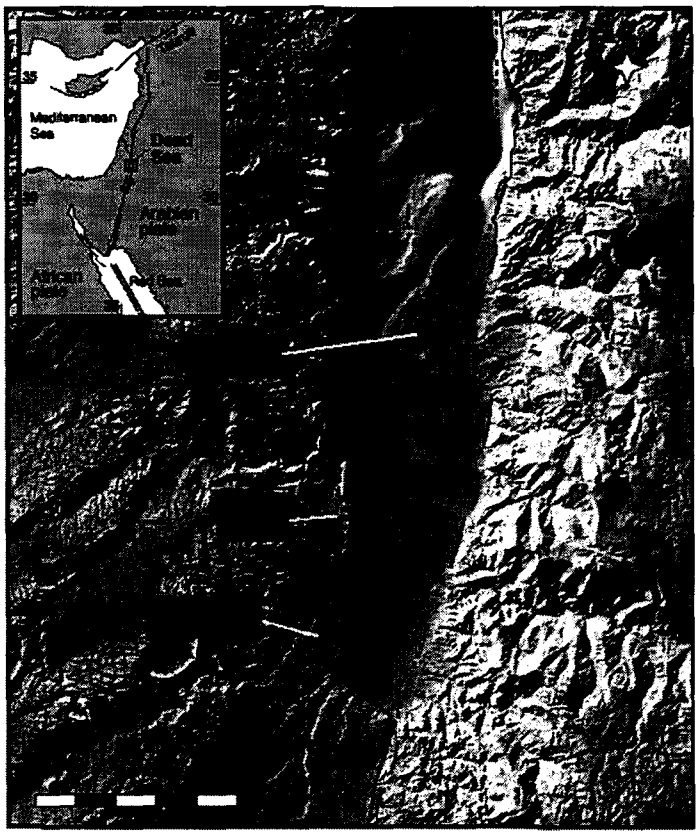

Figure 2
Active tectonic feature in the DSB adapted from Ben-AVRAHAM, 1997; GARFUNKEL, 1997; HALL, 1997; NIEMI and BEN-AVRAHAM, 1997, KLINGER *et al.* 2000b. Background DEM image from HALL (1997).

2. Tectonic Setting of the Dead Sea Area

The Dead Sea Fault (DSF) system is one of the major active strike-slip fault systems of the world. The fault, left-lateral, extends over 1000 km from the Red Sea rift to the Taurus collision zone in Turkey (Fig. 2, inset) accommodating the differential motion between the African and Arabian plates. Its morphology is well-expressed all along strike (GARFUNKEL *et al.*, 1981), with several major linear segments separated by extensional pull-apart basins among which the DSB is the largest. Between 33°N and 35°N the DSF bends eastward, producing large compressional structures responsible for the Lebanon and the Anti-Lebanon mountain ranges. The total offset, south of the Lebanese Range, is estimated to be about 100 km (QUENNELL, 1958; FREUND *et al.*, 1970, GARFUNKEL *et al.*, 1981),

probably posterior to the reorganization of regional tectonics that took place about 15 Myr ago (COURTILLOT *et al.*, 1987). Due to Neogene's extension (FREUND *et al.*, 1968), the DSF zone is marked by a conspicuous rift valley that is particularly well-expressed along the Wadi Araba and the DSB.

The modern slip rate is still in debate. Geological observations, however (mostly south of 33°N) suggest nearly pure left-lateral strike-slip faulting and estimated slip rates range between 1 and 20 mm/yr with preferred values around 5 to 7 mm/yr (FREUND *et al.*, 1968; GARFUNKEL *et al.*, 1981; GARDOSH *et al.*, 1990; GINAT *et al.*, 1998; KLINGER *et al.*, 2000; NIEMI *et al.*, 2001; PE'ERI *et al.*, 2002). BEN MENAHEM (1981) inferred a slip rate of about 2mm/yr from the historical seismicity in the area. By comparison, Nuvel1A (DEMETS *et al.*, 1990) predicts transpressive motion, with 7 mm/yr of left-lateral slip and 6.8 mm/yr of compression for a point located at the DSB.

LE PICHON and GAULIER (1988) has proposed a slip rate of about 9 mm/yr for the Wadi Araba based on gravimetric and magnetic data in the Red Sea. The DSB is about 150 km long to 15 km wide. Layers of low-density sediments fill the basin with a maximum thickness of 10 km (GARFUNKEL and BEN AVRAHAM, 1996). The basin is the largest extensional jog along the DSF, and it is usually described as a pull-apart.

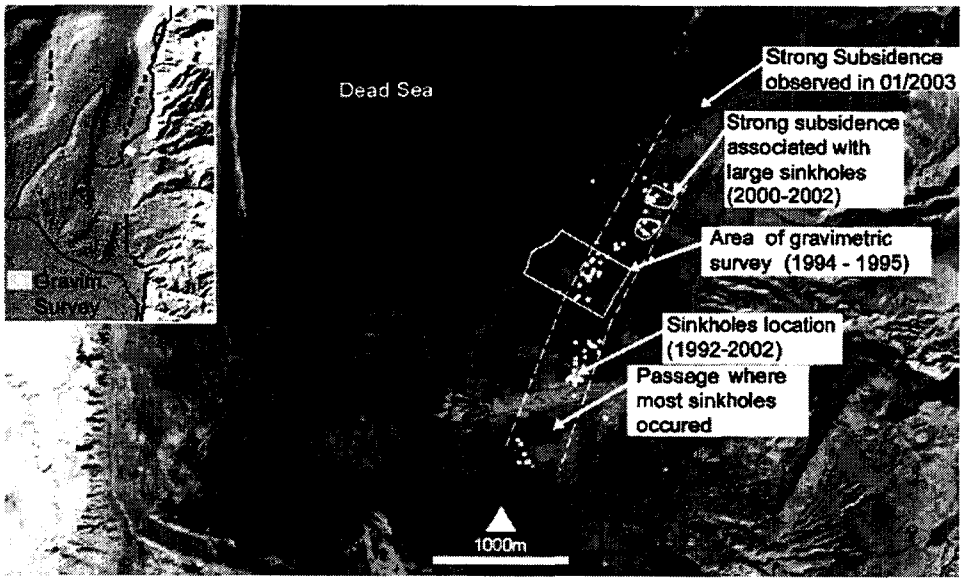

Figure 3
From September 1994 to February 1995, an area of interest was prospected about gravity anomalies. We collected sinkholes information for almost 12 years and mapped it over an Ikonos quick look (20 September, 2000). The almost linear distribution might suggest the phenomenon is tectonically controlled (inset is a subset of Fig. 2).

Inside the DSB, two types of faults, both oriented roughly N-S, can be recognized (Fig. 2). The first set of faults, located mostly offshore, is the continuation of the northern and southern segments of the DSF, forming the pull-apart basin (BEN AVRAHAM, 1997; GARFUNKEL, 1997). Those faults are the main ones accommodating most of the horizontal motion of the DSF. The second set of faults in the area bordering the basin along the western shore, are producing prominent vertical offset easily visible in the topography (GARDOSH *et al.*, 1990; GARFUNKEL *et al.*, 1981). Transverse faults, oriented NNW-SSE, cross obliquely the deep part of the basin. The most conspicuous one is the Khunaizira (or also named Amazyahu) fault, located south of the DSB, with a scarp height of about 50 m. Between these faults, the basin infill is slightly back-tilted toward the South with no large deformations (GARDOSH, 1997; BEN AVRAHAM, 1997). Strong deformations are known only near the diapirs formed by the salt of the Sedom formation. The LP diapir, located just between the northern and the southern basins, is the largest diapir of the DSB. Its geometry is tectonically controlled. Active faults (creating deformations in Holocene sediments) form a secondary basin inside the main one. These faults could be clearly identified from the topography. They are responsible for the sharp edge of the eastern coast of the LP.

3. Subsurface Cavities and Subsidence Areas Detection: Results of Gravimetry and Differential Interferometry in the Ghor Al-Haditha Area

3.1. Gravimetry Measurements and Interpretation

Our reconnaissance campaigns in GAH began in 1989 and were intensified from 1991, in response to the development of a greater number of sinkholes and subsidence areas. Field investigations reinforced the idea that sinkholes in GAH result in most cases from bulky cavities that migrate upwards, sometimes obliquely, by successive collapses of their roofs. When reaching the surface, they generally become, almost spherical, metric to decametric holes. During the geophysical investigations (September 1994 to February 1995), three new sinkholes appeared north of the prospecting zone. Two of them were associated with cracks that evolved quickly to form sinkholes. A third one created a 10-m-deep hole in the middle of a road. Precise gravity measurements are adapted to detect such subsurface cavities (CARA, 1989; AL-MASHAGBAH, 1996; ABOU KARAKI, 1999). However, due to the sensitivity of the instrument and the possible disruptive effects of the variation of topography, we restricted the prospected zone to one of the flattest part of GAH (ABOU KARAKI, 1995).

Fig. 3 shows the investigated area in its context along with the location of sinkholes and two outlines of strong subsidence areas. A new (2003) third large subsidence zone, in rapid expansion, is also mentioned but without precise outline. It

is observed that the distribution of collapse features is not isotropic but is clustering in a 200-m-wide band, with a SSW-NNE direction, suggesting a possible tectonic control of this phenomenon (Fig. 3, inset). The orientation of the band is compatible with the one observed from bathymetric contours few hundred meters North of GAH where a fault has been identified (BEN-AVRAHAM, 1997; GARFUNKEL, 1997; NIEMI and BEN-AVRAHAM , 1997; HALL, 1997).

Fig. 4 shows the set of Negative Residual Bouguer Anomalies (NRBA or anomalies) computed for every measured point by the Griffin method. NRBA essentially reflect the signature of near-surface heterogeneities in the vicinity of a given station. In our area they normally reflect cavities. A cavity will develop into a sinkhole with time. This is why we have more anomalies than sinkholes presently. When comparing the distribution of anomalies and actual collapses between 1995 to 2002, it is observed that several sinkholes occurred in areas where we previously singled out zones as prone to collapse. Fig. 4 compares "significant" (from −0.1

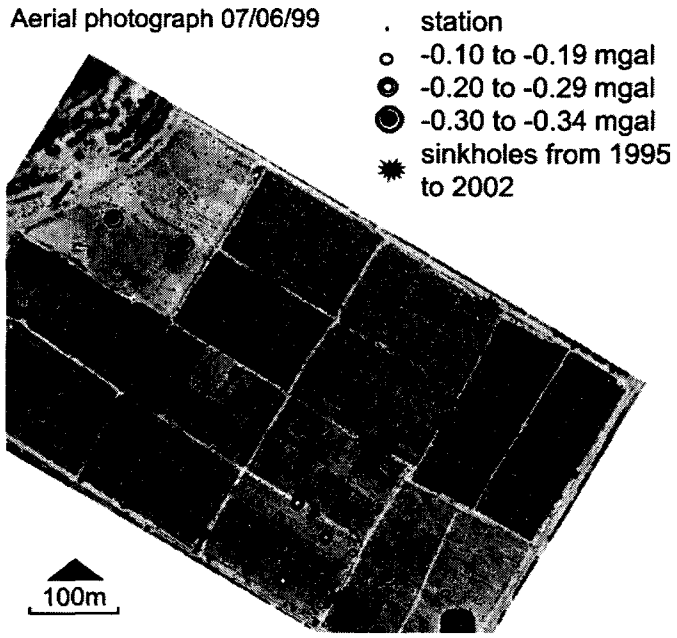

Figure 4
Negative residual Bouguer anomalies detected and localized in a test area (600 m × 300 m) covered by about 800 gravity stations in a regular grid (station spacing = 15 m) . Then, successive sinkholes and subsidence inventory campaigns occurred from 1995 to 2003. Several anomalies had been confirmed in the "passage" (see Fig. 3) indicated by the black dotted lines. We believe that it is just a question of time before other anomalous areas become sinkholes as the system is evolving with time and that anomalous areas inside the 200-m-wide band are most hazardous comparable to anomalous areas elsewhere within the investigated zone.

to −0.34 mGal) anomalies, with our sinkhole database that spread from 1992 to 2003.

The significance of the fact that sinkholes did not appear in the surroundings of negative anomalies detected from both sides out of the 200-m-wide band could be related to one or more, probably a combination, of the following explanations:

The distribution of sinkholes is probably fault-controlled. Faults of various sizes are not unexpected in this well-documented plate boundary environment. This argument is supported by the general correlation between the direction of the distribution of sinkholes in GAH and the general direction of the DS Transform.

Cavities closer to the seashore are less prone to develop into sinkholes as quickly as those elsewhere because the near sea cavities might be totally or partially filled with water which makes their roofs less vulnerable to collapse.

A relation between the collapse timing of the most quickly developing sinkholes and the location of the fresh-water/salt-water interface in the area could not be ruled out.

Several awaited sinkholes occurred a few months to a few years after the survey. They thus confirm the efficiency of our gravimetric approach in detecting prone collapse areas near the DS.

It is easy to carry out modeling of our residual anomalies and translate those into hypothetical sizes, shapes and magnitudes. However, we did not do so because the residual anomalies we computed do not, generally in this area, reflect the signature of a single, simple geometrical source.

From terrain observations and experience, we believe that most of the anomalies reflect multiple sources. In GAH, we observed the fact that filled sinkholes re-opened in the same place, generally within months, which means that cavities and voids are distributed vertically in more than one horizon. Any detected anomaly results, in fact, from the combination of effects of cavities in all horizons, which simply tells us not to expect a simple direct correlation. A 'big' anomaly may result from a small near-surface sinkhole plus a bigger cavity or void in a slightly deeper horizon. Hence, any purely modeling based interpretation would be speculative at best as the interpretation would be a solution to an inverse problem admitting an infinity of mathematically correct solutions (this is of course common to all potential methods).

The results of the gravimetric campaign suggest that the present day sinkhole locations are the ones combining the consequences of subsidence with additional weakness factors, resulting from a particular local hydrogeological or tectonic setting.

The detection of a subterranean void by means of a geophysical measuring device may well indicate the risk of the appearance of a sinkhole. However, the absence of such findings does not totally reject the possibility of future collapses.

A weakness provoked by an initial sinkhole or subsidence will favor more subsidence. This is the effect of subsidence dynamics (the set of phenomena, e.g., tensional cracks, new weakness zones...), provoked by previous gradual subsidence and sinking. As the subsidence dynamics and the continuing drop of the DS water

level govern the phenomena in the particular geological and tectonic setting of the Dead Sea area, it is only a question of time before the occurrence of new sinkholes in, or very near, the areas in which NRBA were detected.

3.2. Subsidence Mapping and Monitoring by Radar Interferometry

In parallel to the field surveys, we applied DInSAR technique from ERS single look complex images to investigate displacement fields in GAH and the northern part of the LP. The phase coherence preservation between two acquisitions is among the basic requirements for an efficient repeat-pass interferometric mapping. To avoid temporal decorrelation, moisture and scatterers distributed over land surface do not change between the time interval that separates two acquisitions (ZEBKER and VILLASENOR, 1992). Consequently, water, wetlands, crops and plantations quickly lose the phase coherence and thus prevent the generation of interferograms. As GAH is a cultivated area, it does not satisfy the basic requirement and DInSAR is difficult to apply for assessing vertical movements there.

BAER *et al.* (2002) realized a differential interferogram for only three months over this area. They wrote "In the sinkhole area of GAH, subsidence of around 30 mm has been observed in the 3-month interferogram. Because it is populated and cultivated, longer-period interferograms of this area are decorrelated".

However, the area mentioned here is not really GAH. It is a mudflat area over the recently emerged shore in the extension of the Wadi Kerak delta, two kilometers west of GAH. Nobody would like to live or work the field in this place. Hence, here, topsoil moisture variation and flash floods most probably control the decorrelation process. Possibilities thus exist to map deformation for few months. The actual GAH probably loses coherence in less than a week because of the density of population and irrigated agriculture that modify topsoil moisture. Only a tandem pair of images preserves coherence over GAH.

The situation is changing in some segments of the passage affected by strong subsidence and sinkholes. Field campaigns, from October 2000 to October 2002, showed two subsidence areas cultivated in 2000 becoming abandoned two years later due to the development of sinkholes and circular concentric large-scale open cracks (Fig. 3). Farmers stopped their exploitation because of collapse threats.

Our field observations in GAH (spreading over more than a decade) showed that subsidence could be an indicator of surfaces that are prone to collapse. This is clearly illustrated by the following example of two comparative pictures, showing the same area in GAH in which subsidence preceded the collapse of seven sinkholes in that area (Fig. 5).

We used GPS to localize open cracks in the topsoil and outline the area covered by Fig. 5 and another area of strong subsidence. In January 2003 we observed a third strong subsidence area in the alignment of the two previous ones (Fig. 3). In all such

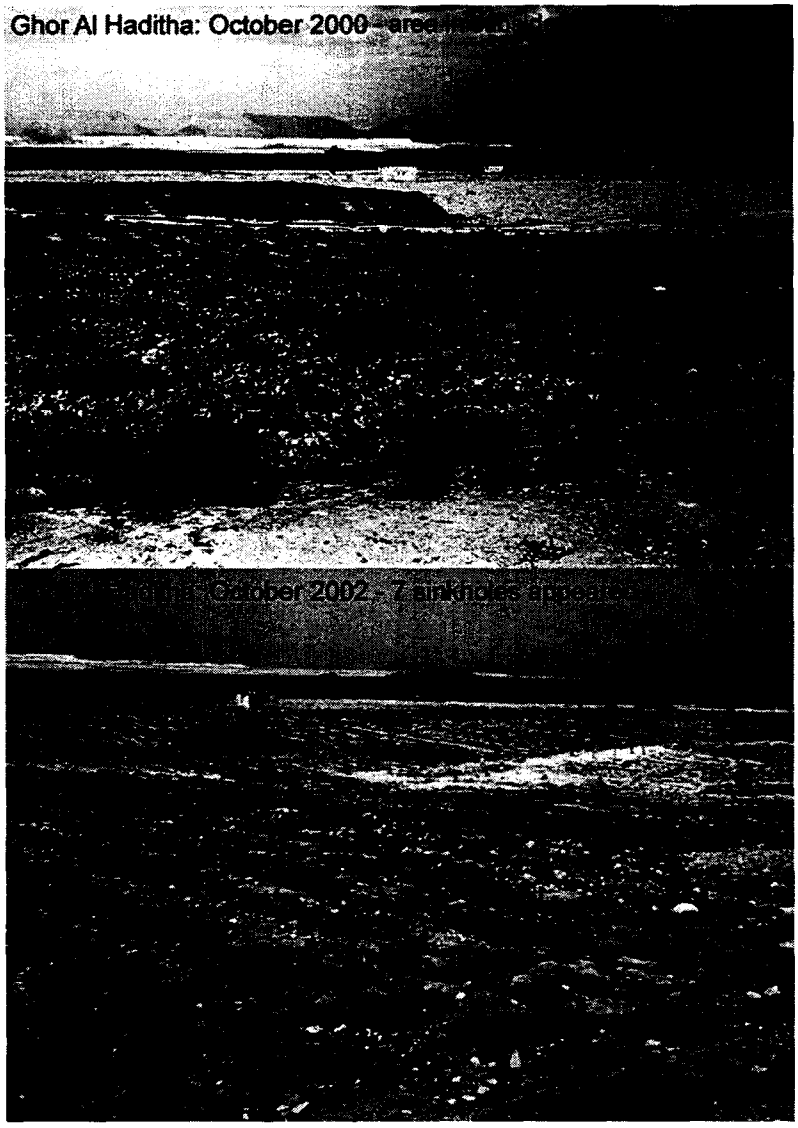

Figure 5
In Ghor Al Haditha, subsidence areas (visible on the photography of October 2000) as large as 200 m in diameter preceded the appearance of major sinkholes (photography of October 2002). The situation became hazardous enough that farmers stopped their agricultural activities.

areas, becoming new natural "no man's lands" and where annual precipitation is less than 50 mm, farmers stopped irrigation and all their agricultural activities. As no temporal decorrelation is expected in such abandoned places, this may allow future measurements by SAR interferometry.

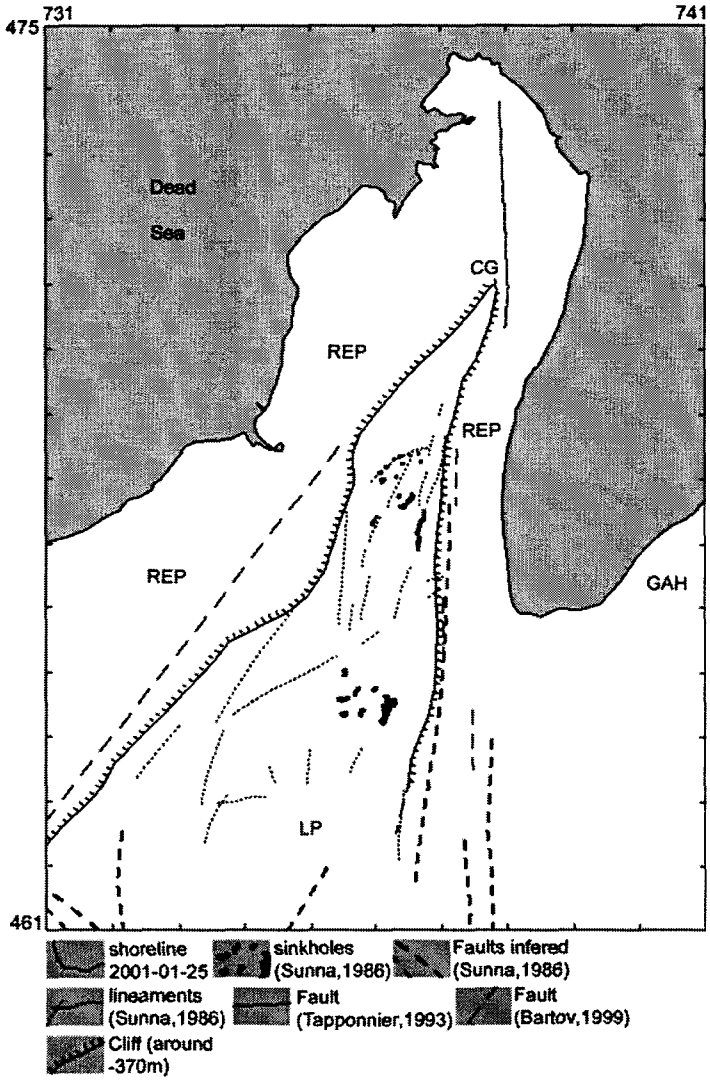

Figure 6
Faults and structures in the northern part of the Lisan Peninsula, along with sources of information. LP = Lisan Peninsula; REP = Recent Emerged Platform; CG = Cape Costigan; GAH = Ghor Al Haditha. (Same abbreviations in the following figures).

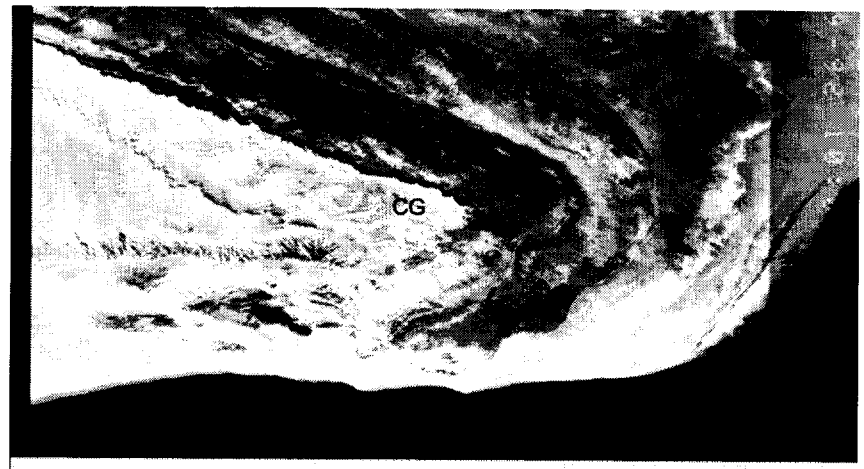
CG

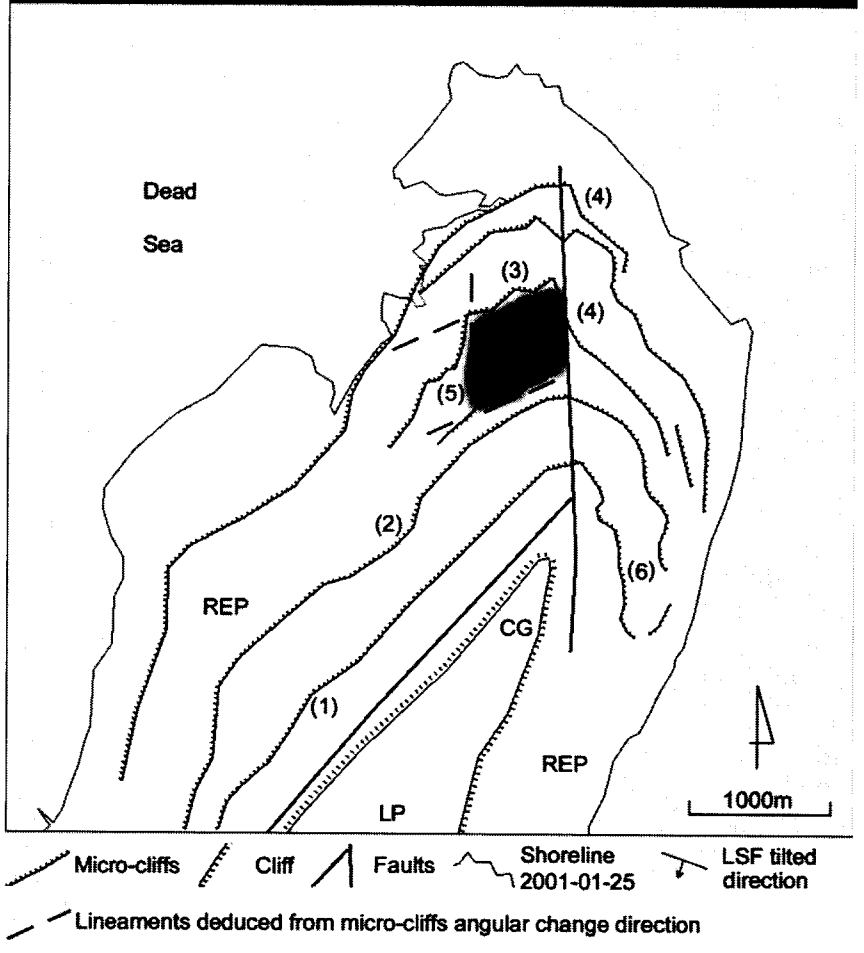
Dead
Sea
(4)
(3)
(4)
(5)
(2)
(6)
REP
CG
(1)
REP
LP
1000m
Micro-cliffs
Cliff
Faults
Shoreline
2001-01-25
LSF tilted
direction
Lineaments deduced from micro-cliffs angular change direction

4. The Lisan Peninsula

4.1. Description of Three Local Fault Networks

Due to the economic importance of the LP, The peninsula was the focus of a number of detailed geological studies. SUNNA (1986), using geological field techniques and 1:25,000 scale aerial photographs, worked out a structural geological map covering the 'old' emerged part of the LP. His map shows two local fault networks, in the N-S and ESE-WNW directions, located respectively in the eastern and southern part of the LP (Fig. 6). A normal offset of the Lisan lake beds by an east dipping, N-S striking fault at the Cape Costigan was observed by TAPPONNIER (1993), who noticed from spot image analysis, the offset of recent salt-rich deposits, which are also apparent on the east side of the Cape.

Moreover, BARTOV (1999) and BARTOV *et al* (2002) mapped a NE-SW listric fault in the western margin of the Lisan with a displacement that he estimated to be larger than 1.5 m. The northern end of the fault segment mapped on Fig. 6 corresponds to the limit of the figure published by BARTOV (1999).

During our field surveys we observed a fault affecting the eastern part of Cape Costigan in the extension of the fault described in BARTOV (1999), Hence, hereafter, we extended that fault all along the western cliff until Cape Costigan.

4.2. Lozenge-Shape feature Outlined from Aerial Photographs

Aerial photographs analysis and field works revealed that the REP can be described as an alternation of micro-cliffs and benches (Fig. 7). A Lozenge-Shape Feature (LSF; CLOSSON *et al.*, 2003) became clearly visible over aerial photographs and satellite images from the end of the eighties when the area emerged. In this place, the geometric relation between micro-cliffs angular change direction and the fault mapped by Tapponnier is particularly obvious.

From this starting observation, we can interpret micro-cliffs local undulations (such as 1 and 2 in Fig. 7) and other strong angular change directions as potential fault activity indicators.

The general orientation of micro-cliffs along the western margin as illustrated in Fig. 7 is SW-NE. Changes occur NNW of Cape Costigan. Micro-cliff contour "3" has an orientation compatible with the one of the fault mapped by Bartov (Fig. 6) after which the orientation changes. We link this change to the activity of the two local fault networks. Comparison between micro-cliff "3" orientation with the fault mapped by Bartov reveals a slight difference, suggesting a clockwise rotation of the LSF.

◄

Figure 7

Top: Stereo color composition reproduced in black and white of two aerial photographs acquired in September 1992. Bottom: Micro-cliffs over the recent emerged platform. LSF = Lozenge-Shape Feature. (Other abbreviations are the same as in figure 6. For the significance of numbers 1 to 6 see text).

Around three to four kilometers north of Cape Costigan, micro-cliffs direction changes again (4). The orientation becomes N-S over several hundred meters and then changes again to become NW-SE. We interpret these strong changes as a consequence of the activity of the N-S local fault.

In the NE sector of Cape Costigan micro-cliffs have an orientation compatible with the N-S local fault network (6).

Gray contrast variations (Fig. 7, (Top) stereo color composition) facilitate mapping the four segments of the LSF (dotted lines). Two of them (4 "east side" and 5 "west side" in Fig. 7) are N-S oriented. The two others ("north" and "south") are NW-SE oriented. Tapponnier (Fig. 6) recognized the eastern segment "4" in the field as a fault. A few hundred meters westward we deduced a lineament parallel to this fault (5).

From aerial photograph interpretation, we believe the LSF is a fault-bounded block slightly tilted toward SW. The outline of the LSF derives from grey contrast variations. Data acquired with other sensors and methods support this interpretation. They are radar coherence images (Fig. 8), InSAR DTM (Fig. 9) and DInSAR subsidence and uplift (Fig. 10). They show elements in agreement with information inferred from aerial photographs.

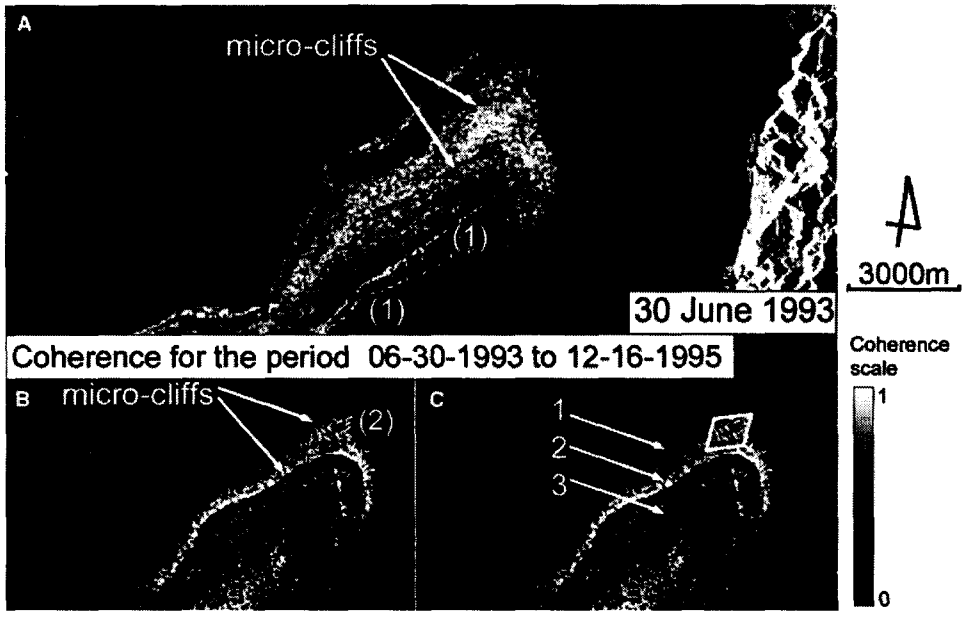

Figure 8
Amplitude (A) and coherence (B and C) images interpretation of the northern part of the Lisan Peninsula ERS images, 30 June 1993 and 16 December 1995, orbit 23105, frame 0621. Images are in slant range projection.

4.3. Contribution of Radar Interferometry to the Geological Background of the Northern Part

Interferometric processing's applied to ERS SAR data brings original information about the REP in three different topics: offset of topsoil deposits which have similar coherence properties, linear topographic variations and deformation fields.

4.3.1. Topsoil offset detected with radar coherence images

The coherence measures the averaged random change of dominant scatterers within a resolution cell (for a particular satellite repeat-pass period). If it exceeds half of the ERS SAR wavelength (28.3 mm) in the direction of slant range, theoretically, it will cause total decorrelation (LIU *et al.*, 2001) and the interferometric phase is pure noise. As a statistical value, coherence does not provide quantitative measurements of the ground scatterers disturbances. Coherence images serve as a measure for the quality of interferograms.

Fig. 8 illustrates the use of coherence data in the mapping of material with similar properties in relation to resistance of topsoil erosion. It presents a radar amplitude subset (A) and a coherence image of the same area (B and C) for a repeat-pass period of 30 months (30 June, 1993 to 16 December, 1995). Grayscale represents coherence values and white color corresponds to surfaces where main scatterers do not change their positions. Over the amplitude image, we note that the 'old' part appears dark (number 1, in white) and the REP is bright (number 2, in black). We reported the same numbers over inset B.

Coherence image shows a white band in the middle of the REP (Fig. 8 C, number 2), sandwiched between two areas of low values (Fig. 8 C, numbers 1 and 3). We examined several other coherence images computed from different image pairs acquired during the nineties. The repeat-pass periods were at least one year. We noted that bands number 1 and 2 had similar behavior in relation to coherence decrease. Respectively they always showed low and high coherence values. On the contrary, band number 3 shows variations of coherence through time. Comparison inside a geographical information system between coherence images and passive remote sensing data indicates that northern and southern limits of band number 2 correspond to micro-cliffs.

The northern limit of band number 2 is a winding line, except two kilometers north of Cape Costigan. At this place, LSF is quite easy to outline over coherence image (Fig. 8C). It suggests offset of rock material with similar properties in relation to resistance of topsoil erosion.

4.3.2. Topographic variations analyzed from insar digital terrain model

We studied an InSAR Digital Terrain Model (DTM; Fig. 9, A) of the northern part of the REP. Ordnance Survey maps point out that the elevation at the bottom of Cape Costigan cliff is –390 m. In December 1995 the DS level was around –409 m

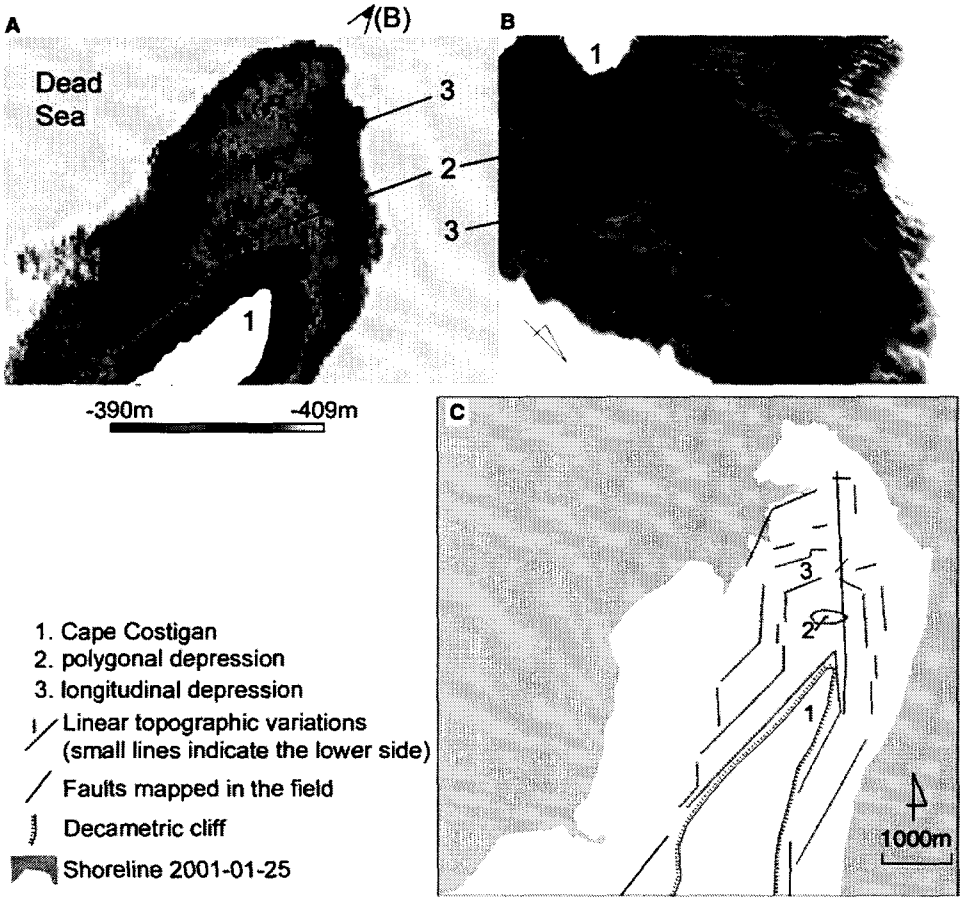

Figure 9
A. Interferogram, 15–16 December 1995, orbit 23105 (ascending), frame 0621, perpendicular baseline 334 m, altitude of ambiguity 33.4 m, resolution 40 m × 40 m; B. Perspective view; C. Lineaments

(USGS, 1998). The difference in elevation over the REP was thus 19 m over a distance of around 3500 m north of Cape Costigan.

In a SAR interferogram, each interferometric fringe border is a contour line and the equidistance is the altitude of ambiguity. To gain knowledge of the lengths, orientations and amplitudes of linear topographic variations ("lineaments") affecting the REP, we first selected one ERS SAR pair acquired with one day interval (15 and 16 December, 1995) to ensure very high coherence and thus accuracy. A wide perpendicular baseline of 334 m was necessary to obtain an altitude of ambiguity of 33.4 m. Hence, the distance from Cape Costigan to the shore is covered by around two thirds of one fringe (19 m in relation to 33.4 m). The elevation accuracy over the

REP in this part of the DTM is between 1 to 2 m and no atmospheric artifacts are present (DERAUW, 1999).

Fig. 9 shows side by side the DTM (A), a perspective view (B) and the inferred map of lineaments (C). A SSE-NNW wide strip of land of relatively 'high' altitudes characterizes the northern part of the REP. We do not observe similar topographic variations over the eastern and western margins. We interpret the strip as a consequence of the intersection between the two local fault networks.

Directions of lineaments are in agreement with the orientation of the two local fault networks. One polygonal depression (Fig. 9, 2) and one longitudinal SW-NE depression (Fig. 9, 3) suggest subsidence areas fault bounded. It is worth while to

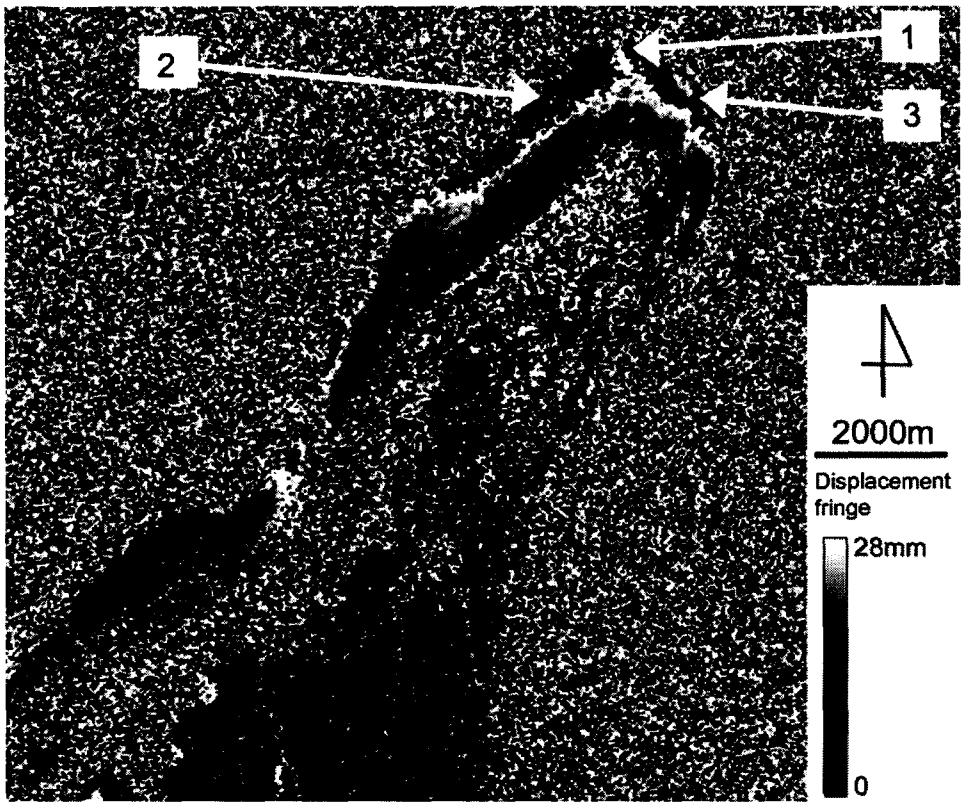

Figure 10
Differential interferograms of the northern part of the LP. Long-term interferogram are made of 15 December, 1995 and 11 October 1997. Topographic reference is the pair of 15 and 16 December 1995 (adapted from DERAUW, 1999). Number 1 is a stable passage between two subsidence areas 2 and 3.

point out that the segment of the collapsed dyke (see also Fig. 1) fits two lineaments revealed by the DTM (Fig. 9, C).

Interpretation inside a geographical information system of an Aster image acquired nine months after the dyke collapse showed a remaining pond of brine precisely located over the polygonal depression number 2. This observation is in agreement with our InSAR DTM values.

The main information inferred from the DTM is that a major part of the SEP 19 was built over a weakness zone probably generated by the interaction between the two local fault networks.

4.3.3. Deformation field mapped by differential sar interferometry

DInSAR mapping of the LP dates back to 1995. Two areas in subsidence were mapped in the northern part (Fig. 10, numbers 2 and 3; DERAUW, 1999). A narrow passage separates them without deformation (Fig. 10, number 1). This stable passage corresponds to the Lozenge-Shape Feature (LSF).

At least three teams mapped similar features (BAER *et al.*, 2002; CLOSSON *et al.*, 2003; SHIMONI *et al.*, 2002). For all teams, the rates of subsidence for the northern part were the highest observed. These rates are summarized in Table 1.

The origin of the subsidence mechanism had been investigated twice from DInSAR data. BAER *et al.* (2002) analyzed the relationships between changes in DS water levels and deformation of the aquifer network. "Calculation of the expected aquifer network consolidation and comparison with InSAR observation confirms that the observed subsidence along the DS shore occurred where the total thickness of the fine-grained marl layers is between 5 and 20 m in the upper 30 m below the surface".

SHIMONI *et al.* (2002) published a "cumulated 93 months vertical deformation map" (between July, 1992 to March, 1999). Those authors noted that "continuing shore subsidence appears along the peninsula margins with maximum value of 44 mm/year in the northern part of the REP between the duration 10/1997–3/1999".

This team suggested that Boqeq fault, located south of the LP, could be the initiating cause of the diapirism deformations detected by interferometry. The uplift in the central dome causes subsidence in its periphery area (as in the northern part of the REP).

Table 1

Subsidence rates in the northern Lisan Peninsula

References	Measured rate of subsidence
BEAR *et al.* (2002)	10–22 mm/yr
SHIMONI *et al.* (2002)	1–15 mm/yr
CLOSSON *et al.* (2003)	18–26 mm/yr

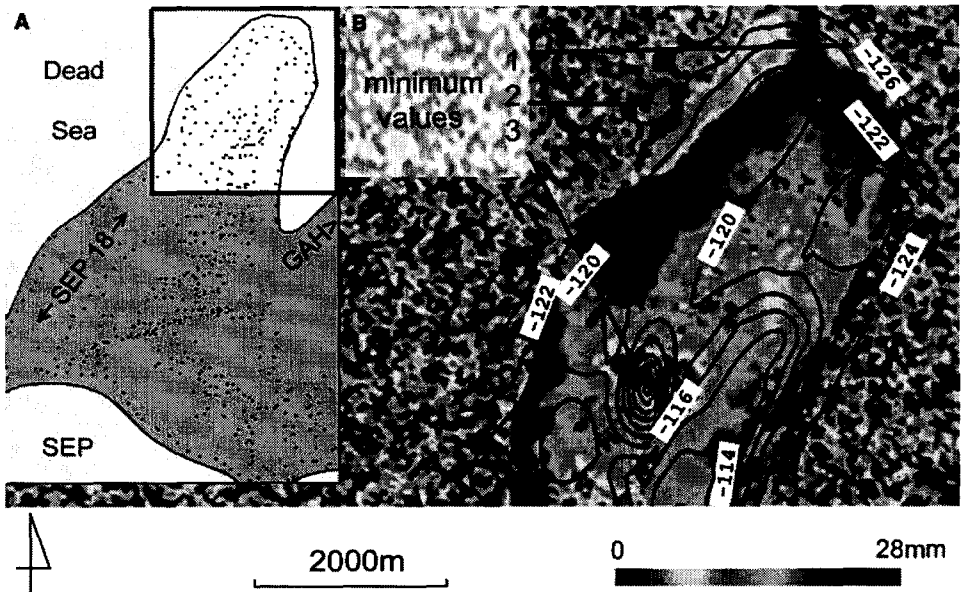

Figure 11
A. Location of the gravity station in 1995–1996 (HUSSEIN, 1997). B. Differential interferogram realized from an ERS pair of images contemporary with the gravimetric campaign (track 078, frame 2979, orbit 21108 for 29-07-1995 acquisition, orbit 6445 for 14-07-1996 acquisition, perpendicular baseline 13m). Differential fringes are visualized with spectrum color palette and negative Bouguer anomalies are in mGal. Topsoil displacements are along the line of sight of the satellite.

4.4. Gravity Measurements and Interpretation

In 1995–96, by gravity measurements (Fig. 11A), HUSSEIN (1997) demonstrated that three absolute minima of the Bouguer anomalies affected the northern part of the LP (Fig. 11B).

The location of the greatest negative Bouguer anomaly (Fig. 11B, minimum value 3; -130 mGal) is in agreement with the "uplifted intermediate zone between the central dome and the Cape Costigan" mapped by SHIMONI *et al.* (2002) over their "cumulated 93 months vertical deformation map."

Two other negative Bouguer anomalies (Fig. 11B, minimum values 1 and 2; -126 mGal and-128 mGal) correspond to subsidence areas along the shore.

Gravimetry and interferometry converge to reflect the same geological elements from two complementary perspectives, i.e. the deficit of mass and the movement respectively. Such approach helps to extrapolate (carefully) differential interferogram in low coherence gaps, as is the case for the collapsed dyke area. As a redundancy exists between the two approaches, the negative Bouguer anomalies strongly suggest an extension for subsidence areas toward NNE and NNW for respectively minimum values 1 and 2 (Fig. 11B).

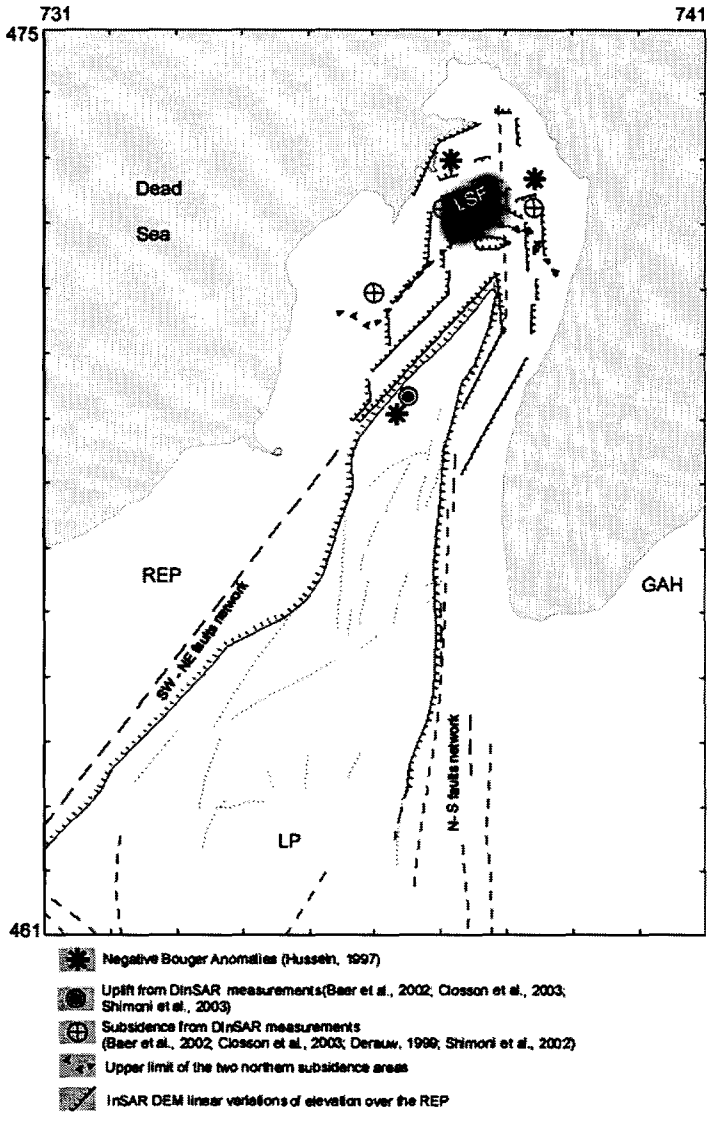

Figure 12
Morpho-structural map of the Lisan Peninsula.(abbreviations are the same as in Fig. 6)

4.5. Morpho-structural Map of the Northern Part

In conclusion of this section devoted to the northern part of the LP, Fig. 12 reproduces the geological facts of Fig. 6 (gray color), added to the main features derived from gravity measurements, InSAR DTM, DInSAR subsidence and uplift (black color).

Fig. 12 shows the destroyed dyke laid down on a zone of negative Bouguer anomaly and where linear small topographic variations are concentrated. Fig. 12 suggests that the N-S and SW-NE fault networks affected the destroyed area. As a possible indicator, the shape of the destroyed zone fits fairly well with lineaments inferred from InSAR DTM.

The LSF is in the center of the northern part of the REP. This structure is partially (could also be completely) fault bounded. Detailed analysis of aerial photographs, passive remote sensing data, radar coherence images, InSAR DTM and deformation fields (DInSAR) of the surrounding area show many other features which suggest fault activity.

All together those data suggest the northern part of the LP as an extremely hazardous zone and still more for major infrastructures such as SEP. We think the collapsed area was one of two high potential risk areas related to the subsidence zones. Our investigations continue the ones of BEAR *et al.* (2002) and SHIMONI *et al.* (2002). The subsidence dynamic could be controlled both by diapirism and the DS water level decrease. We believe that subsidence will continue to threaten SEP 19. Faults and fractures networks are the most hazardous features enhancing collapse possibilities. This is also in agreement with our observations in GAH.

5. Discussion about the Detection, Assessment and Monitoring of Areas Prone to Collapse

5.1. Sinkholes Hazards in Ghor Al Haditha

The detection of places prone to turn into sinkholes implies the creation of an inventory of precursory features characterized by variable scales ranging from topsoil centimetric to decimetric cracks; metric to decametric underground cavities and decametric to hectometric subsidence surfaces.

In GAH, these features are especially characterized by their stage of development and could be detectable by several complementary approaches, i.e., repeated field surveys, geophysical, geodetic and remote sensing techniques including DTM analysis and aerial photographs interpretation.

5.1.1. Stage I: Nucleation and Development of an underground cavity

The smaller the cavity or the deeper it is, makes it the most difficult to detect (but also less hazardous). Areas prone to collapse are (in theory) detectable at this stage by gravimetry, within the limitations of the method, the manner and conditions of its application. The method is generally efficient even before the development of other precursory features. However, practically, only relatively big and/or near surface cavities are easily detectable. Areas prone to collapse are characterized by their negative residual gravimetric anomalies. This is illustrated in Fig. 3.

5.1.2. Stage II: Development of Subsidence Areas

These are detectable, once again in theory, by direct field observations, using geodetic techniques (ideally, time-varying precise leveling). We ruled out this approach because it is very time-consuming and expensive; it could also be hazardous. In favorable size and coherence related conditions, areas of subsidence could be detectable by interferometric techniques.

5.1.3. Stage III, Development of Circular Cracks

The appearance of circular cracks is a strong indication that generally announces the imminence of a cavity roof collapse and the appearance of a new sinkhole. From our investigations and questioning (involving local farmers and inhabitants in GAH), it could be concluded that there is a variety of circular cracks temporal evolution fashions. Some areas with cracks evolve quickly, within a matter of hours to become new sinkholes, others present much slower dynamics. The extreme case is a crack system we detected in the northern part of GAH in 1991. It evolved from a few meters long, 2 cm wide arc of a circle in 1991 to 200 m long and about 0.8 m wide crack by the year 2000. This area marked in Fig. 3 as an area of "Strong subsidence associated with large sinkholes (2000–2002)" became the area of the maximum subsidence in GAH.

It is noteworthy emphasize that a place where sinkholes occur must always be considered as hazardous. We observed that new sinkholes occurred in places where previous collapses existed. This observation indicates that locally, cavities and voids can be distributed vertically in several horizons. Hence, negative residual Bouguer gravity anomalies do not always reflect the signature of a single source but most probably reflect a superposition of multiple sources.

5.2. Dyke Collapse in the Lisan Peninsula

5.2.1. Geotechnical consideration of the SEP 19

We are convinced that the geometrical concordance between the collapsed segment of dyke 19 and one of the most active subsidence areas is not coincidence.

However, we cannot exclude the possibility of problems regarding the design and/or the construction processes of the dyke. Years before the construction of SEP 19, an instrumented trial-fill dyke (about 180 m × 70 m × 12.5 m) was constructed to test and study the engineering characteristics and response of the area's material (AL-HOMOUD *et al.*, 1999). The dyke was built on soft laminated soils of the LP foreshore of the DSB. Geotechnical data were monitored so as to assess the short- and long-term strength of the foundations and to control other geotechnical characteristics.

The conclusion of the study was: "The successful completion of the trial dyke has demonstrated that steep sides up to 12.5 m can be constructed rapidly on the soft laminated soils of the LP foreshore. The construction of the trial dyke has therefore proved to be beneficial to the evaluation of a dyke constructed along the LP shore.

The key factor that makes this fast construction possible is the unexpected very rapid consolidation of the majority of the foundation soils that has been shown to occur." ... "The trial dyke has been stable, pre- and post-construction, because of the well-drained nature of its foundation which prevented the build-up of high pore-water pressures and led to rapid consolidation" (AL-HOMOUD *et al.*, 1999).

Less than three months after the publication of these results, a wide part of the actual 12-km long SEP 19 collapsed and the nearby SEP 18 started facing a series of potentially serious stability threatening problems. We believe these results could hardly be valid in the particular setting of the SEP 19.

Numerous geomorphologic features revealed differences in relation to the whole LP. At first this area is the intersection zone between two local fault networks. Hence, faults and fractures created blocks affected by vertical movements due to either salt diaper uplift or DS water level decrease, and most probably both factors together with different intensities through time.

The filling of the SEP 19 can be described as a key event because it corresponds to the injection of water in highly unstable places. Landslides generally occur after or during a rainy period because unstable areas need lubricant to slide. By comparison, in our case, pumping water injected in the new pond was most probably the triggering factor.

At first glance, the two subsidence areas of the LP could be assessed as less hazardous than the ones observed in GAH because no sinkholes had been observed since their first mapping in 1995. However, their size and shape reflect another kind of hazard, particularly for large infrastructures such as SEPs.

5.2.2. Dinsar Monitoring

Regarding the use of the DInSAR approach, it is important to emphasize that it is only in places where phase is highly preserved (i.e., absence of temporal decorrelation) that deformation field can be mapped. Hence, it is of great interest to understand why coherence remains high or decreases through time over the REP.

Initially we need to know all disruptive factors at the origin of temporal decorrelation, and then reflect as to how we could react toward them. The final goal of this approach is to find a method to artificially extend the high coherence surface in order to map the deformation field everywhere inside the destroyed SEP 19.

Temporal decorrelation of a land surface is dependent on elapsed time between two acquisitions. During this period, topsoil erosion, moisture and human activities are factors able to cause temporal decorrelation. The entire LP is an industrial exploitation zone under the control of the APC that forbids access to the area for non-authorized people. Hence, it is only in particular places that activities are able to affect radar coherence, i.e., quarries of the Cape Costigan, along roads e.g., next to the western cliff and along the shore where dykes were built. We believe that coherence variations through time of band number 3 (Fig. 8C) could be explained by such human activities.

The LP climate is hyper-arid, annual precipitation is less than 50 mm/yr. Consequently, topsoil moisture is non-existent, except very close to the shore. This factor cannot decrease coherence over the LP. As practically no precipitation occurs, only deflation affects the REP topsoil. Wind acts in the same way everywhere. Coherence contrasts are due to resistance variations in relation to the rock material, gravel, sand and dust distribution. LP sediments are subhorizontal. Hence, white band number 2 (Fig. 8C) corresponds to one particular bench of deposits able to preserve coherence for a period greater than two years. It is obviously the contrary for band number 1 (Fig. 8C). Field observations in 1998 showed that powdery material covers the area of band number 1. Such superficial deposits are a consequence of the drying up of the DS.

Since the 1960s, the fresh-water deficit has led to an increase in the salinity of the upper water layers until the density of the upper water mass equaled that of the deep waters. An overturn of the water column resulted at the beginning of 1979 (STEINHORN and GAT, 1983). Thereafter, the chemical properties of the lake changed. The lake is saturated with respect to sodium chloride, and the negative water balance thus caused a mass precipitation of halite. The weight of halite that precipitated between 1976 and 1992 was estimated to be about $2{,}550.10^6$ tons (GAVRIELI, 1997). After this historical event, the sedimentation became finer than previously (SHIMONI, oral communication). Twenty-five years later, the halite deposits are now exposed. The alteration produced a powdery substratum easily transported by the wind.

We presented our understanding of the temporal decorrelation process based upon ERS nineties acquisitions. To map the deformation field until the bottom of the future new dyke with DInSAR technique, we need to solve the problem of the extension westward of the high coherence surface. Hence, we could suggest that the withdrawal of deposits from the high coherent bench to cover the area where topsoil consists of powdery material could be considered. Obviously, DInSAR monitoring should begin just after this operation.

At present, we do not possess a quantitative evaluation of the topsoil erosion during the rapid emptying of the SEP as well as the surface alteration after March 22, 2000. However, we cannot exclude the possibility that band 1 area currently shows topsoil characteristics compatible with long term DInSAR monitoring. To overcome the absence of coherence, other solutions could be tested:

a) We have previously shown the mutual benefits of interferometry complimented with gravimetry. Locally, it seems possible to carefully extrapolate fringes where interferometry is ineffective due to temporal decorrelation.
b) To place several radar reflectors over the dyke. The detection of displacements from radar reflectors had already given valuable results (HARTL *et al.*, 1993).
c) To use radar bands and polarization other than the ERS one (which is C band, VV polarization).

6. Conclusions

We have shown the usefulness of the integrated combination of gravimetry and SAR interferometry data to monitor subsidence zones. For the LP, the deformation field and the significant negative gravity anomalies suggest the presence of a diapiric sub-dome two kilometers SSW of Cape Costigan. We believe that following up and intensifying further interferometric analysis, complemented by other appropriate investigations in specific areas will be of great importance for insuring or later monitoring the stability of the particularly exposed segments of the whole existing set of dykes as well as future ones.

The field of negative gravity anomalies helped to complete the missing part of the DInSAR deformation field for the subsidence areas.

Regarding GAH, the temporal decorrelation due to human activities prevented efficient mapping with the DInSAR approach in most of the affected part. Nevertheless, this problem could be solved by the fact that farmers are progressively stopping agricultural activities in the most dangerous parts of their exploitations.

Conventional terrestrial geophysics can be effective in limited areas. However, this approach alone is not adapted for large areas as it is very time and effort consuming and in certain cases, highly hazardous too. For the Jordanian DSB environment, such an approach is quite unsuited to solve the regional problem. An adequate answer at this scale could be provided by a well-planned and specially designed rational use of space techniques that ensures overcoming the temporal decorrelation problem in the SAR interferometry domain. In the framework of necessary future monitoring of the LP, and indeed, of the whole DSB Jordanian shore, which is increasingly undergoing ambitious development of its tourist and cultural potential, zones of interest or subsidence areas could be monitored by SAR interferometry where coherence is maintained either naturally or artificially through the use of reflectors.

Acknowledgements

Appreciation is expressed to Dr. Majdi Barjous of the Jordanian Natural Resources Authority for fruitful discussions and to Dr. Fathi Shaqour- University of Jordan for critically reading the manuscript. The Deanship of scientific research, University of Jordan, supports the work of Najib Abou Karaki while the Walloon Region (First University Program) and the Royal Military Academy support that of Damien Closson. We thank Christian Barbier (Centre Spatial of Liege) for reviewing an earlier version of this paper.

The Work of Prof. Najib Abou Karaki was done in the framework of the European Community supported project APAME "Archeoseismology and Paleoseismology for the protection of Cultural Heritage and Archaeological sites in the Middle East, The Impact of Large Earthquakes on the Archeological sites and

cultural Heritage in the Middle east (Jordan, Lebanon, Syria, and Turkey)" ICA3-CT 2002-10024.

References

ABOU KARAKI, N. (1999), *Geoelectrical and precise gravity surveys for the detection of underground cavities in the test zone of the Khalifa city site, Abu Dhabi.* Centre for Consultations Technical Services and Studies, University of Jordan, 50 pp. (Done for the Rabah Engineering Laboratories Est., Abu Dhabi, United Arab Emirates.)

ABOU KARAKI, N. (1995), *The gravity survey: Assessment of the hazard of subsidence and sinkholes in Ghor Al-Haditha area—Final report.* In El-Isa *et al.*, Centre for Consultation, Technical Services and Studies, University of Jordan, unpublished, pp. 117–124.

AL-ARAB AL YAWM (2001), *1329, Jan. 9*, is a Jordanian daily newspaper (in Arabic), Amman.

AL-HOMOUD, A., MAKINSON, C., TAL, A. B., and PENMAN, J.G. (1999), *In-Situ Geotechnical Experimentation and Stability Evaluation of an Instrumented 180 m × 70 m × 12.5 m Fill Dyke Constructed on Laminated Soft Ground,* Environ. Geology *39* (2), 177–196.

AL-MASHAGBAH, A. (1996), *Application of Precise Gravity Techniques in Detecting Cavities for Civil Engineering Purposes*, M.Sc. Dissertation, University of Jordan- Amman (in English).

ARKIN, Y. and GILAT, A. (2000), *Dead Sea Sinkholes—an Ever-developing Hazard.* Environm. Geology *39*, 711–722.

BAER, G., SCHATTNER, U., WACHS, D., SANDWELL, D., WDOWINSKI, S., and FRYDMAN, S. (2002), *The Lowest Place on Earth is Subsiding—An InSAR (Interferometric Synthetic Aperture Radar) Perspective*, Geolog. Soc. Am. Bull. *114* (1), 12–23.

BARTOV, Y. (1999), *The Geology of the Lisan Formation in Massada Plain and the Lisan Peninsula* Ph.D. Dissertation, Institute of earth Science, The Hebrew University of Jerusalem, 60 pp. (in Hebrew).

BARTOV, Y., STEIN, M., ENZEL, Y., AGNON, A., and RECHES, Z. (2002). *Lake Levels and Sequence Stratigraphy of Lake Lisan, the Late Pleistocene Precursor of the Dead Sea,* Quaternary Res. *57*, 9–21.

BATAYNEH, A., AL-ZOUBI A., and HASSOUNEH, M. (1995), *Magnetic and Gravity Investigations of Lisan Peninsula—Dead Sea (Jordan)*, J. China Univ. Geosci. *6* (2), 213–218.

BEN-AVRAHAM, Z., *Geophysical framework of the Dead Sea: Structure and tectonics.* In *The Dead Sea, The Lake and its Setting* (eds. Tina M. Niemi *et al.*) (Oxford University Press, 1997) pp. 22–35.

BEN-MENAHEM, A. (1981), *Variation of Slip and Creep along the Levant Rift over the Past 4500 Years,* Tectonophysics *80*, 183–197.

CARA, M., *Géophysique* (Dunod-Bordas, Collection Géosciences, Paris, 1989).

CLOSSON, D., ABOU, KARAKI, N., HANSEN, H., DERAUW, D., BARBIER, C., and OZER, A. (2003), *Space-borne Radar Interferometric Mapping of Precursory Deformations of a Dyke Collapse-Dead Sea Area-Jordan.* Intern. J. Remote Sensing *24* (4), 843–849.

COURTILLOT, V., ARMIJO, R., and TAPPONNIER, P. (1987), *The Sinai Triple Junction Revisited,* Tectonophysics *141*, 151–168.

DEMETS, C., GORDON, R.G., ARGUS, D. F., STEIN, S. (1990), *Current plate motions,* Geophys. J *101*, 425–478.

DERAUW, D. (1999), *Phasimétrie radar à synthèse d'ouverture: théorie et applications*, Doctorate, Liege University, Belgium, 121 pp. (In French).

FREUND, R., ZAC, I., and GARFUNKEL, Z. (1968), *Age and Rate of the Sinistral Movement along the Dead Sea Rift,* Nature *342*, 637–642.

FREUND, R., GARFUNKEL, Z., ZAK, I., GOLDBERG M., WEISBROD T., and DERIN B. (1970), *The Shear along the Dead Sea Rift,* Philosoph. Trans. Roy. Soc. London *267*, 107–130.

GARDOSH, M., RECHES, Z., and GARFUNKEL, Z. (1990), *Holocene Tectonic Deformation along the Western Margins of the Dead Sea,* Tectonophysics *180*, 123–137.

GARDOSH, M., KASHAI, E., SALHOV, S., SHULMAN, H., and TANNENBAUM, E., *Hydrocarbon exploration in the southern Dead Sea area*, In *The Dead Sea, The Lake and its Setting* (eds. Tina M. Niemi, Ben-Avraham Z., and Gat J.) (Oxford University Press, 1997) pp. 57–72.

GARFUNKEL, Z., *The history and formation of the Dead Sea basin*, In *The Dead Sea, The Lake and its Setting* (eds. Tina M. Niemi, Ben-Avraham, Z., Gat, J.) (Oxford University Press, 1997) pp. 36–55.

GARFUNKEL, Z. and BEN AVRAHAM, Z. (1996), *The Structure of the Dead Sea Basin*, Tectonophysics *266*, 155–176.

GARFUNKEL, Z., ZAK, I., and FREUND, R. (1981), *Active Faulting in the Dead Sea Rift*, Tectonophysics *80*, 1–26.

GAVRIELI, I. (1997), *Halite deposition from the Dead Sea: 1960–1993. In The Dead Sea: The Lake and Its Setting* (eds. Niemi, T. M., Ben-Avraham, Z., and Gat, J.) (Oxford University Press, New York, 1997), pp. 161–170.

GINAT, H., ENZEL, Y., and AVONI, Y. (1998), *Translocated Plio-Pleistocene Drainage Systems along the Arava Fault of the Dead Sea Transform*, Tectonophysics *284*, 151–160.

HALL, J. K., *Topography and bathymetry of the Dead Sea depression*. In *The Dead Sea, The Lake and its Setting* (eds. Tina M. Niemi, Ben-Avraham, Z., and Gat, J.) (Oxford University Press, 1997) pp. 11–21.

HARTL, PH., THIEL, K.H., WU, X., and XIA, Y. (1993), *Practical application of SAR interferometry; experiences made by the Institute of Navigation*, Proceed. the Second ERS-1 Symp., Hamburg, Germany.

HASSOUNEH, M (1997), *Structure of the Lisan Peninsula of the Dead Sea basin from gravity analysis*, Natural Resources Authority, Geophysical Department, Amman, 30 pp.

HUSSEIN M. J. (1997), *Gravitational and Magnetic Study of the Lisan Area—Southern Dead Sea*, M.Sc. Thesis, University of Jordan, 138 pp.

KLINGER, Y., AVOUAC, J.P., ABOU KARAKI, N., DORBATH, L., BOURLES, D., and REYSS, J. L. (2000), *Slip-rate on the Dead Sea Transform Fault in Northern Araba Valley (Jordan)*, Geophys. J. Internat. *142*, 3, 769–782.

KNIGHT, D. J. (1993), *Extension west of Lisan Peninsular sinkholes along access road*, The Arab Potash Company, DJK/A110/92235B, unpublished Report. 16 pp.

LE PICHON, X., GAULIER, J.M. (1988), *The Rotation of Arabia and the Levant Fault System*, Tectonophysics *153*, 271–294.

MCKENZIE, D., DAVIES, D., and MOLNAR, P. (1970), *Plate Tectonics of the Red Sea and East Africa*, Nature *226*, 243–248.

LIU, J. G., BLACK, A., LEE, H., MOORE, J. M., and HANAIZUMIS, H. (2001), *Land Surface Change Detection in a Desert Area in Algeria Using Multi-temporal ERS SAR Coherence Images*, Internat. J. Remote Sensing *22*, 13, 2463–2478.

NIEMI, T.M. and BEN-AVRAHAM, Z., *Active tectonics in the Dead Sea basin*. In *The Dead Sea, The Lake and its Setting* (eds. Tina M. Niemi, Ben-Avraham, Z., and Gat, J.) (Oxford University Press, 1997) pp. 73–87.

NIEMI, T., ZHANG, H., ATALLAH, M., and HARRISON, J. B. (2001), *Late Pleistocene and Holocene Slip Rate of the Northern Wadi Araba fault, Dead Sea Transform, Jordan*. J. Seismol. *5*, 449–474.

PE'ERI, S., WDOWINSKI, S., SHTIBELMAN, A., BECHOR, N., BOCK, Y., NIKOLAIDIS, R., and VAN DOMSELAAR, M. (2002), *Current Plate Motion across the Dead Sea Fault from Three Years of Continuous GPS Monitoring*. Geophys. Res. Lett. *29*,14,42-1–42-4.

QUENNELL, A. (1958), *The Structural and Geomorphic Evolution of the Dead Sea Rift*, Quarterly J. Geol. Soc. of London *114*, 1–24.

SALAMEH, E. and ABU NASEIR, T. (1999), *The Quantitative and Qualitative Impacts of the Rehabilitation of the Municipal Water Supply Network on the Groundwater Resources in Amman Area, Jordan*, J. Hydrogeol. Environ, *18*, 189–197.

SALAMEH, E. and EL-NASER, H. (1999), *Does the Actual Drop in Dead Sea level Reflect the Development of Water Sources within its Drainage Basin?* Acta Hydrochemica et Hydrobiologica *27*, 5–11.

SALAMEH, E. and EL-NASER, H. (2000), *Changes in the Dead Sea Level and their Impacts on the Surrounding Groundwater Bodies*, Acta Hydrochemica et Hydrobiologica *28*, 2–33.

SHIMONI, M., HANSSEN, R.F., VAN DER MEER, F., KAMPES, B. M., and BEN DOR, E. (2002), *Salt Diapir Movements Using SAR Interferometry in the Lisan Peninsula, Dead Sea Rift*, Proc. SPIE *4543*, 151–160.

STEINHORN, I. and GAT, J., (1983), *The Dead Sea*, Scientific Am. *249 (October)*, 84–91.

SUNNA, B. F. (1986), *The geology of salt deposits in the Lisan Peninsula-Dead Sea, Seminar on Salt in the Arab world, Ministry of Energy and Mineral Resources*, NRA, Amman–Jordan, 4-6 May.

TAPPONNIER, P. (1993), *Collapse hazard near projected dyke west Lisan Peninsula-Dead Sea*, The Arab Potash Company Project, unpublished Report. 19 pp.

TAQIEDDIN, S.A., ABDERAHMAN, N.S. and ATTALAH M. (2000), *Sinkhole Hazards along the Eastern Dead Sea Shoreline Area, Jordan: A Geological and Geotechnical Consideration*, Environ. Geology *39* (11), 1237–1253.

USGS, compiled by the United States Geological Survey for the Executive Action Team, Middle East Water Data Banks Project, *Overview of Middle East Water Resources* (Jordanian Ministry of Water and Irrigation, Palestinian Water Authority, Israeli Hydrological Service, 1998. ISBN 0-607-91785-7.

ZEBKER, H.A., and VILLASENO, R, J. (1992), *Decorrelation in Interferometric Radar Echoes*, IEEE Transaction in Geosciences and Remote Sensing *30* (5), 950–959.

(Received April 10, 2003, accepted November 11, 2003)